PLOS Climate

RESEARCH ARTICLE

# Ontogeny of dwarf tropical cyclones in the western North Pacific

**Seungwoo Yoo**[1], **Chang-Hoi Ho**[1,2*], **Minhee Chang**[3,4], **Jinwon Kim**[2], **Changhyun Yoo**[2]

**1** School of Earth and Environmental Sciences, Seoul National University, Seoul, Korea, **2** Department of Climate and Energy Systems Engineering, Ewha Womans University, Seoul, Korea, **3** Environmental Planning Institute, Seoul National University, Seoul, Korea, **4** Climate Tech Center, Seoul National University, Seoul, Korea

* hoch@ewha.ac.kr

Check for updates

OPEN ACCESS

**Citation:** Yoo S, Ho C-H, Chang M, Kim J, Yoo C (2026) Ontogeny of dwarf tropical cyclones in the western North Pacific. PLOS Clim 5(4): e0000885. https://doi.org/10.1371/journal.pclm.0000885

**Editor:** Jingyu Wang, Nanyang Technological University, SINGAPORE

**Received:** December 5, 2025

**Accepted:** March 12, 2026

**Published:** April 8, 2026

**Copyright:** © 2026 Yoo et al. This is an open access article distributed under the terms of the Creative Commons Attribution License, which permits unrestricted use, distribution, and reproduction in any medium, provided the original author and source are credited.

**Data availability statement:** The Joint Typhoon Warning Center best track is publicly available in the Western North Pacific Ocean Best Track Data repository, https://www.metoc.navy.mil/jtwc/jtwc.html?western-pacific. The ERA5 pressure-level datasets analyzed in this study are available in the Copernicus Climate Data Store repository at https://doi.org/10.24381/

## Abstract

Destructive tropical cyclones (TCs) have recently been observed to develop despite strong vertical wind shear and cause catastrophic damages. This study investigates the properties of dwarf (or shallow) TCs which form under strong-shear conditions (≥ 13 m $s^{-1}$) at the time of genesis, using 444 TCs over the western North Pacific for the period 2003–2022. The TCs are stratified by vertical wind shear magnitude to explore the climatology of TCs at genesis. The dwarf TCs generally have shorter life spans and weaker peak intensities compared to the normal TCs formed in weak-shear environments. The dynamics governing the dwarf and normal TC genesis are compared by analyzing the terms in the azimuthally-averaged tangential wind tendency equation. The difference between the dwarf and normal TCs occurs in the mean terms of the equation: the mid-tropospheric mean outflow of absolute vorticity and the vertical transport of the tangential wind gradient are stronger in the dwarf TCs than the normal TCs. Ultimately, the strong inward low-tropospheric winds in dwarf TCs enhance their tangential winds, causing the near-surface wind to reach 17 m $s^{-1}$, the TC threshold.

## Introduction

Tropical cyclones (TCs) are largely perceived to develop in weak vertical wind shear (VWS) conditions; however, some TCs can form and persist in the presence of strong VWS. In the North Atlantic basin, major hurricane Ian in 2022, one of the most destructive landfalling TCs on record, began as a tropical depression at 0600 UTC 23 September when the environmental deep-layer (200–850 hPa) VWS was as strong as 14 m $s^{-1}$ [1, 2]. Similarly, in the western North Pacific, super typhoon Haishen in 2020 was under VWS of ≥ 15 m $s^{-1}$ when it first attained the tropical storm intensity at 0000 UTC 1 September [2]. Both TCs managed to overcome initially adverse strong VWS conditions to become intense TCs as soon as the VWS decreased to low-to-moderate values. These TCs highlight the need to better understand TC genesis under high VWS conditions.

cds.bd0915c6. The OI SST dataset is available at https://www.ncei.noaa.gov/products/optimum-interpolation-sst. The JRA-3Q dataset is available at https://doi.org/10.20783/DIAS.645.

**Funding:** This work was funded by the Korea Meteorological Administration Research and Development Program under Grant RS-2023-00236880 (to SY, CHH, and JK) and supported by the Specialized University Program for Confluence Analysis of Weather and Climate Data of the Korea Meteorological Institute (to CHH and CY).

**Competing interests:** The authors have declared that no competing interests exist.

The environmental VWS is a critical factor in the genesis and intensification of TCs. TC development is favored when the deep-layer VWS is weak as weak VWS allows efficient transport of water vapor from the lower troposphere to the upper troposphere [3–5]. On the other hand, strong VWS inhibits TC genesis due to strong ventilation and subsequent intrusion of dry air caused by the separation of low-level and upper-level circulations, i.e., vortex tilt [6]. Typically, TC genesis and/or intensification are prevented when the magnitude of the deep-layer VWS exceeds 11–12.5 m $s^{-1}$ [7–9]. When the VWS is moderate, i.e., neither too weak nor too strong, other factors such as the vortex and convection structures, ambient humidity and sea-surface temperatures determine the eventual development or non-development of a TC [10–12].

The processes of governing the intensification of TCs under moderate VWS have been identified in previous observational and numerical studies. [13] used idealized ensemble TC simulations to show that the onset time of TC intensification under moderate VWS is strongly related to the magnitude of the downshear-left vortex tilt. Relatively weak TCs such as tropical storms, also experience low-level vortex reformation near the mid-troposphere [14, 15], allowing for more compact and vertically oriented TCs [16]. Increases in upshear precipitation and vortex alignment [13, 17, 18], which facilitate the symmetrization of TC precipitation, are also found to be associated with increased TC intensification rates. Upper-level outflows induced by the TC itself can sometimes mitigate the negative effects of VWS, especially when the shear is concentrated in the upper troposphere [19, 20].

Less attention has been paid to the genesis of TCs in high-shear environments. TCs capable of intensifying in moderate-to-strong shear conditions are already accompanied by maximum sustained winds of at least 17 m $s^{-1}$ prior to encountering such an environment [14,15,20–23]. To the authors' knowledge, the formation of TCs under strong VWS conditions, with maximum sustained winds increasing from below to above 17 m $s^{-1}$, has not yet been documented in previous literature. This is probably because TCs are less vertically stacked and thus more susceptible to the negative effects of VWS (e.g., precipitation asymmetry and dry air intrusion) in their formation stages than in their mature states [24–26].

This study aims to unravel the story behind such TCs that develop despite strong VWS. The climatological and dynamical characteristics of strong-shear TC genesis over the western North Pacific, in contrast to weak-shear cases, are revealed through the lifetime TC properties stratified by initial VWS and the azimuthally-averaged tangential wind tendency equation, respectively. Although this equation has been used to explain the intensification of individual TCs after reaching 17 m $s^{-1}$ [27–30], here it is extended to TCs and their composites at the genesis stage for the first time, as far as the authors are aware.

## Data and methodology

### Data

The best track data from the Joint Typhoon Warning Center are used to determine the genesis of TCs in the western North Pacific (0°–50°N, 100°E − 180°) during the

period 2003–2022 [31]. The best track data include the best estimate of a TC's position, the maximum wind speed, the minimum pressure, and intensity at six-hour intervals, derived from observations and numerical model outputs during and after the progression of the TC. A total of 484 tropical disturbances attained tropical storm (TS) status, or maximum sustained winds of at least 17 m $s^{-1}$ (= 34 kt) during the period analyzed. The genesis time of a TC is defined as the time when the TC first reached TS status according to the Joint Typhoon Warning Center best track. However, there are differences in the TS designations among the best track datasets produced by different forecast agencies. In particular, the Regional Specialized Meteorological Center of the western North Pacific located in Tokyo, Japan does not recognize 40 of the 484 systems as TSs. Therefore, we analyze the remaining 444 TCs that are classified as TS by both the Joint Typhoon Warning Center and the Regional Specialized Meteorological Center.

Gridded pressure-level meteorological fields are obtained from the 0.25° × 0.25° fifth generation European Centre for Medium-range Weather Forecasts Reanalysis (ERA5) dataset [32], to analyze the statistical and dynamical properties of dwarf and normal TC formations. The zonal and meridional wind fields, vertical velocity, relative vorticity, and geopotential height of 27 pressure levels from 1000 to 100 hPa are used as the pressure-level variables [33].

Daily optimum interpolation (OI) sea surface temperature (SST) version 2.1 fields [34, 35] are used to calculate the SSTs in the vicinity of a TC. The OI SST dataset is a long-term record of SSTs dating back to September 1981 that incorporates multiplatform observations into a 0.25° × 0.25° grid. This dataset is used in place of the ERA5 SST, as ERA5 relies on different external SST sources before and after September 2007 [32], a transition that occurs within the study period. The environmental SST of a TC is defined as the grid-point average of OI SST within 500 km of the best-track center.

### Methodology

The VWS has traditionally been calculated as the magnitude of the environmental horizontal wind difference between 200 hPa and 850 hPa [3,36,37], i.e., VWS = $\sqrt{(u_{200}-u_{850})^2+(v_{200}-v_{850})^2}$, where $u$ and $v$ represent the wind speed in the zonal and meridional directions, respectively, and the subscripts indicate the pressure level (in hPa). The environmental winds of a TC at a pressure level, and subsequently the VWS are determined by averaging the ERA5 grid-point horizontal winds within 500 km of the TC center according to the best track data. Recent studies have attempted to remove the effects of the TC circulation by either excluding the core region of the TC or applying vortex removal methods before calculating the VWS [37,38]. However, the strong-shear TC samples obtained from the original method are mostly not excluded by applying such methods; rather, the TC removal produces some artificial results that make further dynamical analyses difficult. Therefore, TCs are not removed in calculating the environmental winds in this study. Moreover, since most strong-shear TCs show uniformly increasing VWS with height at the time of genesis (S1 Fig), no distinction is made between the lower- and upper-level VWS.

Statistical significance of the differences in climatological properties between TCs forming under strong and weak VWS is evaluated using the Kruskal–Wallis and Wilcoxon rank-sum tests [39, 40]. The Kruskal–Wallis test is used for multiple independent groups to determine whether there exists a group that originates from a different distribution. The one-sided Wilcoxon rank-sum test is used in this study for testing whether one population tends to have smaller values than the other. P-values for the Wilcoxon rank-sum test are calculated with the exact probabilities given in [40].

The azimuthally-averaged tangential wind tendency equation [27–30] in cylindrical pressure coordinates can be written as

$$\frac{\partial \overline{v}}{\partial t} = \underbrace{-\overline{u}\left(\overline{\zeta}+f\right)}_{V_{m\zeta}} \underbrace{-\overline{\omega}\frac{\partial \overline{v}}{\partial p}}_{V_{mv}} \underbrace{-\overline{u'\left(\zeta'+f'\right)}}_{V_{e\zeta}} \underbrace{-\overline{\omega'\frac{\partial v'}{\partial p}}}_{V_{ev}} + \overline{F_\lambda},$$

where the overbars and primes denote the mean and eddy components, respectively, and $u$, $v$, $\zeta$, $f$, $\omega$, $p$, and $F_\lambda$ are the radial wind, tangential wind, relative vorticity, Coriolis parameter, pressure vertical velocity, pressure, and friction, respectively. The first two terms on the right-hand side, $V_{m\zeta}$ and $V_{mv}$, represent the mean radial transport of absolute vorticity

and the mean vertical transport of the tangential wind gradient, respectively, while the third and fourth terms, $V_{e\zeta}$ and $V_{ev}$, are each the eddy counterparts of $V_{m\zeta}$ and $V_{mv}$, respectively. These four terms are calculated by transforming the zonal and meridional winds at each pressure level to radial and tangential winds, and then bilinearly interpolating the variables in the four terms (except $f$, which is directly proportional to the sine of latitude) onto a polar grid with 5-km radial and 2° azimuthal increments. The TC center is defined as the best-track position at all pressure levels, as the average tilt magnitude differences between strong-shear and weak-shear TCs are found to be negligible (S1 Table, [41]). The friction term is neglected in this study because the ERA5 dataset does not provide the necessary variables for its computation.

## Results

### Climatology of TCs stratified by VWS at the time of genesis

The climatological characteristics of the lifetimes of 444 western North Pacific TCs in 2003–2022 are categorized according to the VWS magnitude at the time of genesis (Fig 1). TCs are classified into five categories according to VWS: VWS < 4 m s$^{-1}$, 4 m s$^{-1}$ ≤ VWS < 7 m s$^{-1}$, 7 m s$^{-1}$ ≤ VWS < 10 m s$^{-1}$, 10 m s$^{-1}$ ≤ VWS < 13 m s$^{-1}$, and VWS ≥ 13 m s$^{-1}$. The number (percentage) of TCs in each category is 125 (28.2%), 151 (34.0%), 107 (24.1%), 44 (9.9%), and 17 (3.8%), respectively. The percentage of TCs developing in moderate to strong VWS of at least 10 m s$^{-1}$ is considerably lower than that calculated using all TC intensities in a previous study [7], where about 25% of TCs in the western North Pacific experience VWS of at least 10 m s$^{-1}$. This supports the notion that pre-formed TCs are more susceptible to VWS than mature TCs [24].

Life span of the TCs formed in strong VWS is generally much shorter than those formed in weaker VWS (Fig 1a). The median duration of TCs in the VWS < 4 m s$^{-1}$ category is 126 h, but it decreases to 72 h for VWS ≥ 13 m s$^{-1}$. When the analysis is extended to the first and third quartiles (Fig 1a), the difference between the strong-shear and weak-shear TCs at the genesis is more evident. The longevity of TCs does not vary much with VWS when VWS < 13 m s$^{-1}$; the first (third) quartile fluctuates between 60 h and 84 h (150 h and 180 h). However, in the VWS ≥ 13 m s$^{-1}$ category, the quartile value noticeably decreases to 18 h (90 h). These differences are statistically significant at the 95% confidence level according to the Kruskal–Wallis test among the five VWS ranges ($p = 0.0039$) and the one-sided Wilcoxon rank-sum tests comparing the VWS ≥ 13 m s$^{-1}$ category with the VWS < 4 m s$^{-1}$ ($p = 3.1 \times 10^{-4}$) or VWS < 13 m s$^{-1}$ ($p = 3.9 \times 10^{-4}$) categories. Thus,

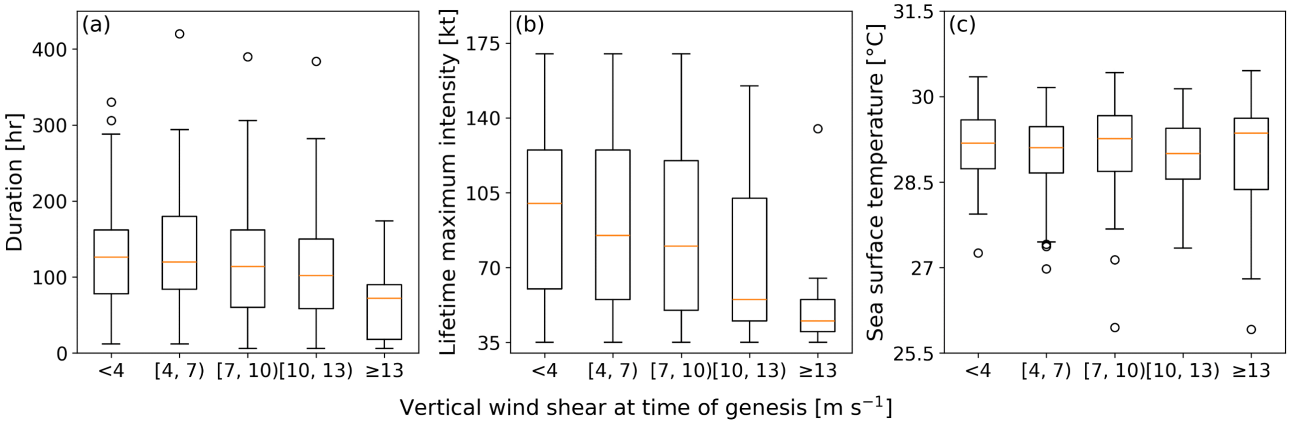



**Fig 1. Climatological characteristics of TCs according to environmental vertical wind shear.** (a) Duration (units in h), (b) lifetime maximum intensity (units in kt), and (c) underlying sea surface temperature (units in °C) of the western North Pacific tropical cyclones during 2003–2022 stratified by the environmental deep-layered vertical wind shear at the time of genesis. The upper, middle, and lower bars in the box indicate the 75% (Q3), median, and 25% (Q1) values. The upper and lower whiskers indicate Q3 + 1.5×(Q3 − Q1) and Q1 − 1.5×(Q3 − Q1), respectively.

https://doi.org/10.1371/journal.pclm.0000885.g001

even if high-shear TCs can form, they last shorter than low-shear TCs regardless of subsequent large-scale environmental conditions.

The lifetime maximum intensity also decreases with the VWS at the time of genesis (Fig 1b). The median (first quartile) intensity decreases steadily from 100 kt (60 kt) in the VWS < 4 m $s^{-1}$ category to 45 kt (40 kt) in the VWS ≥ 13 m $s^{-1}$ category. Using the third quartile values, the TCs under strong shear at the genesis can be easily distinguished from those less affected by shear. The third quartile of the lifetime maximum intensity ranges between 100 kt and 125 kt when the VWS is less than 13 m $s^{-1}$, but it drops abruptly to 55 kt when VWS exceeds 13 m $s^{-1}$. In fact, only two TCs reached the typhoon grade (≥ 64 kt), one of which barely crossed the threshold. The Kruskal–Wallis test results on the five VWS ranges ($p = 2.4 \times 10^{-7}$) indicate that there exists a group of TCs with stochastically different lifetime maximum intensity. Moreover, the lifetime maximum intensity of VWS ≥ 13 m $s^{-1}$ TCs are statistically smaller than the other four categories with 95% confidence ($p = 3.9 \times 10^{-7}$, $9.2 \times 10^{-7}$, $2.0 \times 10^{-4}$, and 0.023 for the VWS < 4 m $s^{-1}$, 4 m $s^{-1}$ ≤ VWS < 7 m $s^{-1}$, 7 m $s^{-1}$ ≤ VWS < 10 m $s^{-1}$, 10 m $s^{-1}$ ≤ VWS < 13 m $s^{-1}$ categories, respectively). This suggests that the final peak intensity of a TC may be limited by its initial environmental VWS [42].

SST at the time of genesis is not critical in differentiating strong VWS formation from normal TCs at the 95% confidence level (Fig 1c; $p = 0.25$ according to the Kruskal–Wallis test). SSTs of at least 26.5°C are known to be an important necessary thermodynamic condition for TC genesis [3,43–45]. This is confirmed in Fig 1c, where all but two of the 444 western North Pacific TCs meet this condition. However, the correlation between SSTs and the initial VWS is statistically insignificant ($r = -0.076$, $p = 0.11$). The first and third quartiles, as well as the median, are all between 28.3°C and 29.7°C regardless of the VWS range. While the median SST is highest in the VWS ≥ 13 m $s^{-1}$ category at 29.4°C, the interquartile range is also the largest of the VWS bins at 1.25°C, which is 27% larger than the next largest interquartile range in the 7 m $s^{-1}$ ≤ VWS < 10 m $s^{-1}$ category at 0.98°C. These results necessitate the analysis of other factors including the dynamics of TCs to discern the characteristics of TC genesis under strong shear.

### Comparison of dynamic forcing between dwarf and normal TCs

The four main terms of the azimuthally-averaged tangential wind tendency equation, $V_{m\zeta}$, $V_{mv}$, $V_{e\zeta}$, and $V_{ev}$ (see Methodology) are computed for the 17 cases in the VWS ≥ 13 m $s^{-1}$ category (hereafter dwarf TCs) at the time of genesis. The first two terms, $V_{m\zeta}$ and $V_{mv}$, each refer to the mean radial transport of absolute vorticity and the mean vertical transport of the tangential wind gradient, while $V_{e\zeta}$ and $V_{ev}$ are the eddy counterparts of $V_{m\zeta}$ and $V_{mv}$, respectively. The mean terms computed for the dwarf TCs are compared with those of the remaining 427 cases, or normal TCs. The eddy terms, $V_{e\zeta}$ and $V_{ev}$, are not discussed in this section as the differences between the two classifications are not statistically significant (see Summary and discussion).

The magnitudes of $V_{m\zeta}$ and its constituents, radial wind ($\overline{u}$) and absolute vorticity ($\overline{\zeta_a} = \overline{\zeta} + f$), are calculated for both the normal and dwarf TCs (Fig 2). $V_{m\zeta}$ in dwarf TCs shows marked differences from the normal TCs (Figs 2a, b). Normal TCs show consistently negative $V_{m\zeta}$ in the upper troposphere, around 200–300 hPa, outwards to at least 500 km (Fig 2a). However, in dwarf TCs, the magnitude of upper-tropospheric $V_{m\zeta}$ is somewhat smaller than the normal TCs; instead, negative $V_{m\zeta}$ is prominent in the mid-troposphere, namely 400–600 hPa (Fig 2b). It is also noteworthy that the magnitude of the low-tropospheric $V_{m\zeta}$ exceeds 25 m $s^{-1}$ $day^{-1}$ in both the dwarf and normal TCs; these values are the largest of the terms in this analysis.

The shallow nature of dwarf TCs may explain the differences in their $V_{m\zeta}$ distribution from the normal TCs. For the normal TCs, there is an inflow layer in the lower troposphere below 800 hPa and a strong outflow in the upper troposphere above 300 hPa (Fig 2c). A large absolute vorticity of ≥ $1.8 \times 10^{-4}$ $s^{-1}$ extends to about 300 hPa (Fig 2e), indicating that the vorticity is vertically stacked into the upper troposphere. On the other hand, the upper-tropospheric outflow of the dwarf TCs is significantly weaker than that of the normal TCs; instead, there is a secondary outflow level in the mid-troposphere near 500 hPa (Fig 2d). The absolute vorticity near the center of the dwarf TCs is significantly weaker than that of the

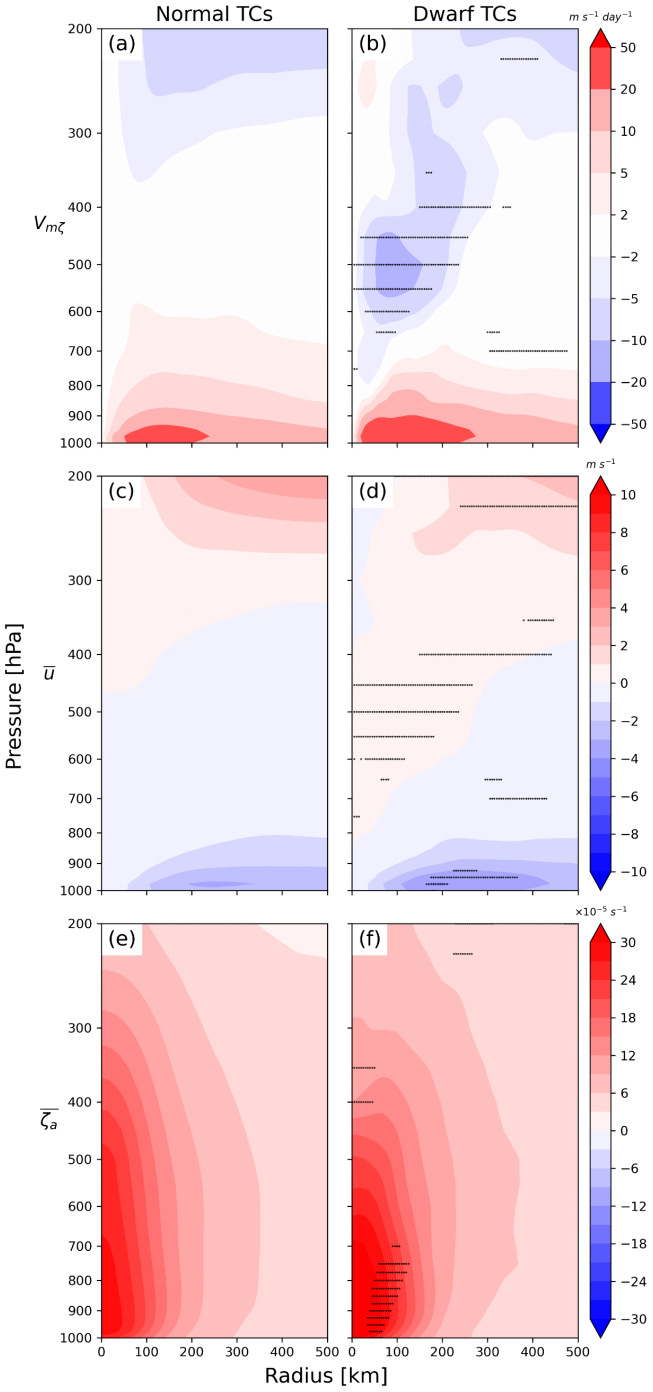



**Fig 2. The radial-vertical composites of the mean radial transport of absolute vorticity $\mathbf{V}_{m\zeta}$ and its components at the time of genesis.** (a, b) $V_{m\zeta}$ (units in m s$^{-1}$ day$^{-1}$), (c, d) mean radial wind ($\overline{\mathbf{u}}$, units in m s$^{-1}$), and (e, f) mean absolute vorticity ($\overline{\zeta_a}=\overline{\zeta}+\boldsymbol{f}$, units in $10^{-5}$s$^{-1}$) observed in (a, c, e) normal and (b, d, f) dwarf TCs at the time of genesis. Differences between the dwarf and normal TCs in each term that are statistically significant at the 95% confidence level according to the two-sided t-test are shown as black dots in the right panels.

https://doi.org/10.1371/journal.pclm.0000885.g002

normal ones in the 300–400 hPa level, indicating a less vertically stacked system (Fig 2f). These observations indicate that the depths of the secondary circulation in normal TCs are deep even in their formation stage, but those in dwarf TCs are shallow.

$V_{mv}$ and its component variables—vertical velocity ($\overline{\omega}$) and pressure gradient of the tangential wind ($\partial\overline{v}/\partial p$)—are also compared between normal and dwarf TCs (Fig 3). $V_{mv}$ slopes outwards with height and is more vertically dispersed in the dwarf cases than in the normal cases (Figs 3a, b). The magnitude of $V_{mv}$ above 500 hPa within 100 km of the center decreases to close to 0 m $s^{-1}$ $day^{-1}$ (Fig 3b), in contrast to the TCs under weaker shear where it remains mostly positive regardless of pressure level. Also, the largest values of $V_{mv}$ are extended from 300 to 700 hPa, compared to the weaker-shear cases where they are confined in the 200–400 hPa range.

The vertical distribution of $V_{mv}$ in normal and dwarf TCs may reflect whether the low-level tangential winds propagate into the upper troposphere. In normal TCs, the vertical velocity within 100 km of the TC center points upward throughout the troposphere, with large values of $5 \times 10^{-3}$ Pa $s^{-1}$ persisting in the mid- (650 hPa) to upper troposphere (250 hPa) (Fig 3c). The tangential wind does not decrease much until the 300-hPa level (Fig 3e) to allow the vertical transport of tangential winds into the upper troposphere. Meanwhile, in dwarf TCs, the region of upward vertical velocity is tilted outwards and is concentrated in the low- to mid-troposphere from 800 to 400 hPa, while it almost disappears near the center above 500 hPa (Fig 3d). The tangential wind below the boundary layer about 200 km from the center increases faster than the normal TCs and decreases from 700 to 450 hPa (Fig 3f). The level of the negative tangential wind gradient partially coincides with that of the outflow, indicating divergence near the 500 hPa level. This indicates that, in the high-shear cases, strong low-level winds decrease in the middle levels and do not propagate into upper levels.

Consequently, the vertical depth of the axisymmetric component of TCs ($V_{m\zeta}$ and $V_{mv}$) under strong-shear environments is very shallow at the time of genesis and extends only up to the mid-levels near 500 hPa. In particular, the outward motion at 500 hPa, the reduced vertical motion near the center above 500 hPa, and the absence of tangential wind propagation into the upper troposphere point to the shallow, or "dwarf" secondary circulation of highly sheared TCs.

Enhanced radial winds are observed in dwarf TCs at least 12 h before TC genesis (Fig 4). At 12 h before genesis, the maximum low-level inflow (below 850 hPa) is about 3.5 m $s^{-1}$ for the dwarf TCs, while it is close to 2.6 m $s^{-1}$ for the normal TCs (Figs 4a, b). Statistically significant differences in the radial wind, at the 95% confidence level, are found around the 950 and 975 hPa levels 180–380 km from the center. Six hours later, or six hours before genesis, the radial wind difference between the dwarf and normal TCs increases (Figs 4c, d). Large swaths of statistically-significant stronger low-level winds are observed in the dwarf TCs compared to the normal TCs, with the maximum inflow remaining $< 3$ m $s^{-1}$ in the former and $> 4$ m $s^{-1}$ in the latter. These differences persist up to the genesis time, although the magnitude of the low-tropospheric inflow remain similar and the range of significantly stronger inflow in the dwarf TCs, relative to the normal TCs, is mainly confined to the 950 hPa level (Figs 4e, f). The enhanced radial winds in the lower troposphere and the subsequent tangential wind increase via the azimuthally-averaged tangential wind tendency equation may lead the near-surface sustained wind speed to reach the threshold required for TC designation, 17 m $s^{-1}$.

## Summary and discussion

Understanding the characteristics of TC formations under strong-shear conditions is crucial in filling the current knowledge gap in TC genesis. This study investigates 444 TCs that formed in the western North Pacific during 2003–2022 to analyze the susceptibility of TCs to VWS in the genesis stage. The majority of the TCs that formed in strong VWS (>13 m $s^{-1}$) environment (or dwarf TCs) do not persist long or intensify to typhoon strength (≥ 64 kt), highlighting the importance of initial environmental conditions on subsequent developments of TCs. SSTs, one of the most important factors in TC genesis, cannot differentiate the TC formation in strong-shear conditions from that in lesser-shear conditions. Rather, the two types of TC formation are dynamically distinguished by the patterns of two terms in the azimuthally-averaged tangential wind tendency equation: the mean radial transport of absolute vorticity and the mean vertical transport of the tangential wind

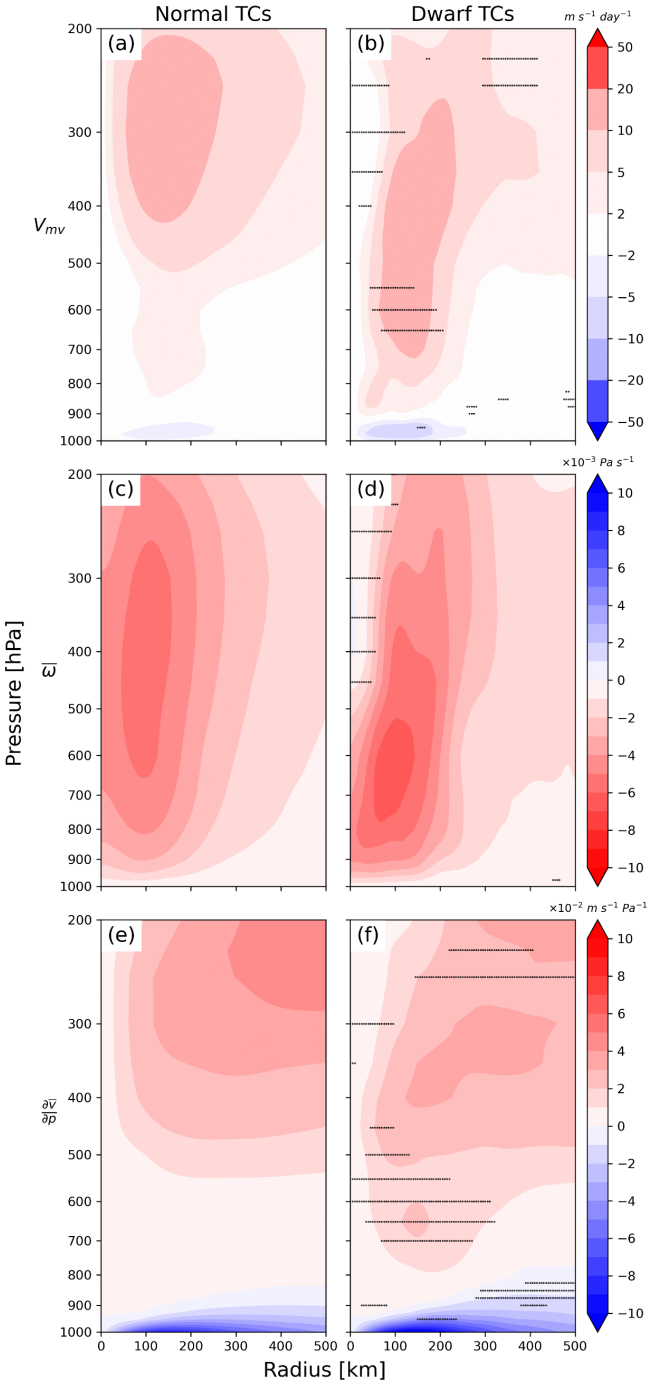



**Fig 3. The radial-vertical composites of the mean vertical transport of tangential wind gradient $V_{mv}$ and its components at the time of genesis.** (a, b) $V_{mv}$ (units in m s$^{-1}$ day$^{-1}$), (c, d) pressure vertical velocity ($\overline{\omega}$, units in $10^{-3}$ Pa s$^{-1}$), and (e, f) tangential wind gradient ($\partial\overline{\boldsymbol{v}}/\partial\boldsymbol{p}$, units in $10^{-2}$ m s$^{-1}$ Pa$^{-1}$) observed in (a, c, e) normal and (b, d, f) dwarf TCs at the time of genesis. Differences between the dwarf and normal TCs in each term that are statistically significant at the 95% confidence level according to the two-sided t-test are shown in black dots on the right panels.

https://doi.org/10.1371/journal.pclm.0000885.g003

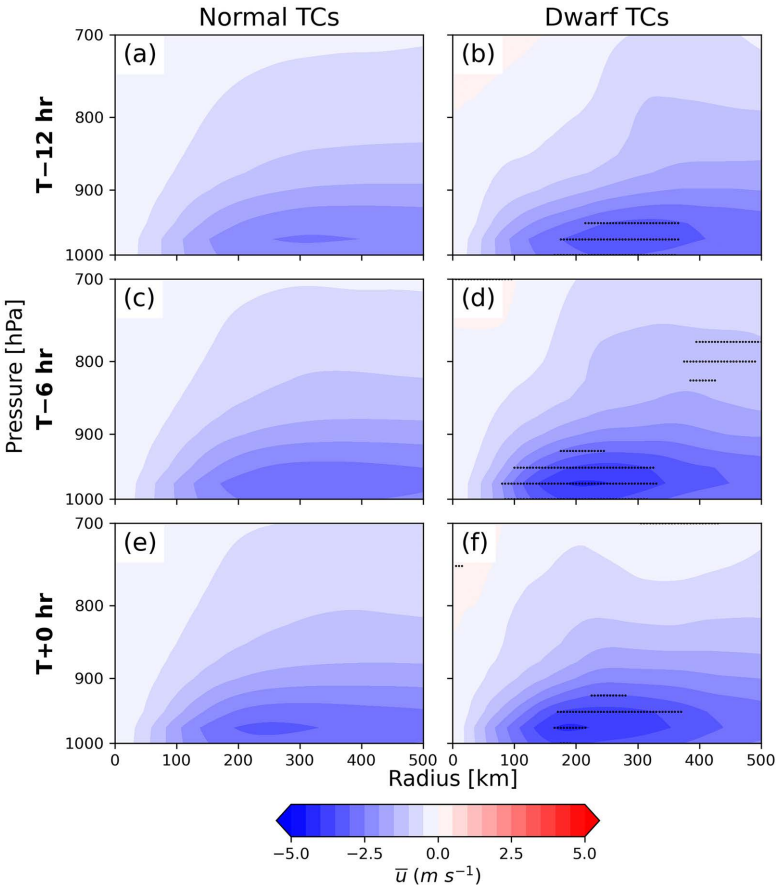



**Fig 4. Short-term evolution of radial winds ($\bar{u}$) in normal and dwarf TCs.** 1000–700 hPa radial winds (units in m $s^{-1}$) observed (a, b) 12 h before genesis, (c, d) 6 h before genesis, and (e, f) at the time of genesis in normal (a, c, e) and dwarf (b, d, f) TCs. Differences between the dwarf and normal TCs in that are statistically significant at the 95% confidence level according to the two-sided t-test are shown in black dots on the right panels.

https://doi.org/10.1371/journal.pclm.0000885.g004

gradient. Further examination of the two terms suggests that the dwarf TCs have a shallower secondary circulation than the normal TCs, hence the name “dwarf”.

This study confirms the existence of TCs that reach TS intensity—the stage at which the systems become self-sustaining—even under strong VWS [3]. It is noted that these cases should be distinguished from pre-TC disturbances that initially endure strong VWS but only develop into TCs after the VWS weakens to low-to-moderate levels [5, 46, 47].

The structure of the eddy terms, $V_{e\zeta}$ and $V_{ev}$, does not vary significantly between the dwarf and normal cases (S2 Fig). In both cases, negative values of $V_{e\zeta}$ extend up to 200 hPa within 200 km from the low-level center before turning positive. Positive values of $V_{ev}$ extend up to 400 hPa and the sign changes to negative above this level. While the maximum absolute value of $V_{e\zeta}$ in the dwarf cases exceeds 20 m $s^{-1}$ $day^{-1}$, noticeably different from the normal TCs, it is not statistically significant at the 95% confidence level. Whether or not the magnitude of the eddy terms plays a role in the genesis of dwarf TCs is beyond the scope of this study.

Enhancement of the radial wind in dwarf TCs may increase the near-surface winds to reach the 17 m $s^{-1}$ TC threshold. The radial wind is a component of $V_{m\zeta}$ in the azimuthally-averaged tangential wind tendency equation. Given that the absolute vorticity is mostly positive regardless of TC types, stronger inflows or negative radial winds induce larger $V_{m\zeta}$,

which in turn increases the tangential wind tendency. This leads to increases in both the radial and tangential winds over time, with 950 hPa winds of ≥ 17 m $s^{-1}$ in dwarf TCs 6 h before genesis (S3 Fig). Further analysis is needed to verify the causes of the surface wind increase.

The analysis in this study is mainly based on the dynamical variables observed at the time of genesis according to the Joint Typhoon Warning Center best track. Additional large-scale factors are used to distinguish the dwarf TCs from the normal TCs, such as the environmental flow surrounding the TCs [48, 49] or the geographical location of the TCs. However, these factors do not vary with VWS.

The ERA5 dataset is used to compute the terms in the azimuthally-averaged tangential wind tendency equation. The implementation of different reanalysis data is known to cause some quantitative discrepancies in tropospheric winds [50]. However, the main results of this study are not sensitive to the dataset used as repeating the analysis using the Japanese Reanalysis for Three Quarters of a Century [51, 52] yields essentially identical results as reported in this study (S4–7 Figs). Moisture variables, such as mid-tropospheric relative humidity, latent heat, and convective activity are also known to influence genesis [3, 53–55]. However, they are not analyzed using the reanalysis data in this study because they are sensitive to subgrid-scale processes. High-resolution model simulations can be useful for analyzing the thermodynamic factors involved in dwarf TC genesis in future studies.

Results of this study present the characteristics of dwarf TCs over a 20-year period from a statistical point of view and focus on differentiation of dwarf TCs from normal TCs using composites. In this respect, the characteristics of individual TCs may be obscured. For instance, a small subset of normal TCs could potentially be reclassified as dwarf TCs if the classification is based on vertical size instead of VWS. Furthermore, climatic variability may have played a role in the analyzed period considering that the first dwarf TC exceeding 65 kt was observed only recently, in 2020 (TC Haishen, Fig 1a). Due to the scarcity of dwarf TCs, analyses of such changes are challenging, but should be further investigated.

## Supporting information

**S1 Fig. Vertical profile of vertical wind shear in dwarf tropical cyclones.**
(TIF)

**S2 Fig. The radial-vertical composites of the eddy terms in the azimuthally-averaged tangential wind tendency equation.** (a, b) $V_{e\zeta}$ and (c, d) $V_{ev}$ observed in (a, c) normal and (b, d) dwarf TCs at the time of genesis (units in m $s^{-1}$ $day^{-1}$). Differences between the dwarf and normal TCs in each term that are statistically significant at the 95% confidence level according to the two-sided t-test are shown as black dots in the right panels. The formulations of each term are presented in the Methodology section.
(TIF)

**S3 Fig. Same as Fig 4 but for tangential winds.**
(TIF)

**S4 Fig. Same as Fig 2 but using the JRA-3Q dataset.**
(TIF)

**S5 Fig. Same as Fig 3 but using the JRA-3Q dataset.**
(TIF)

**S6 Fig. Same as Fig 4 but using the JRA-3Q dataset.**
(TIF)

**S7 Fig. Same as S2 Fig but using the JRA-3Q dataset.**
(TIF)

**S1 Table. Mean tilt magnitude of TCs stratified by magnitude of vertical wind shear.** P-values of each bin are computed based on the two-sample independent t-test with respect to dwarf TCs.
(DOCX)

## Author contributions

**Conceptualization:** Seungwoo Yoo, Chang-Hoi Ho.

**Formal analysis:** Seungwoo Yoo, Minhee Chang.

**Investigation:** Seungwoo Yoo.

**Methodology:** Seungwoo Yoo, Changhyun Yoo.

**Supervision:** Chang-Hoi Ho.

**Validation:** Seungwoo Yoo, Chang-Hoi Ho, Minhee Chang, Changhyun Yoo.

**Visualization:** Seungwoo Yoo, Minhee Chang.

**Writing – original draft:** Seungwoo Yoo, Chang-Hoi Ho.

**Writing – review & editing:** Seungwoo Yoo, Chang-Hoi Ho, Jinwon Kim.

## References


1. Bucci LL, Alaka L, Hagen A, Delgado S, Beven J. Tropical cyclone report: Hurricane Ian (AL092022). Miami (FL). 2023. https://www.nhc.noaa.gov/data/tcr/AL092022_Ian.pdf
2. Sampson B, Chirokova G, DeMaria G, Dostalek J, Kaplan J, Knaff J, et al. Statistical tropical cyclone intensity forecast technique development. Fort Collins (CO): Regional and Mesoscale Meteorology Branch. 2024. https://rammb2.cira.colostate.edu/research/tropical-cyclones/ships/#DevelopmentalData
3. Gray M. Global view of the origin of tropical disturbances and storms. Mon Wea Rev. 1968;96(10):669–700. https://doi.org/10.1175/1520-0493(1968)096<0669:GVOTOO>2.0.CO;2
4. McBride JL, Zehr R. Observational analysis of tropical cyclone formation. Part II: Comparison of non-developing versus developing systems. J Atmos Sci. 1981;38(6):1132–51. https://doi.org/10.1175/1520-0469(1981)038%3C1132:OAOTCF%3E2.0.CO;2
5. Chang M, Ho CH, Chan JCL, Park MS, Son SW, Kim J. The tropical transition in the western North Pacific: The case of tropical cyclone Peipah (2007). J Geophys Res Atmos. 2019;124(10):5151–65. https://doi.org/10.1029/2018JD029446
6. DeMaria M. The effect of vertical shear on tropical cyclone intensity change. J Atmos Sci. 1996;53(14):2076–88. https://doi.org/10.1175/1520-0469(1996)053<2076:TEOVSO>2.0.CO;2
7. Zehr RM. Tropical cyclogenesis in the western North Pacific. Washington (DC): National Environmental Satellite, Data, and Information Service, National Oceanic and Atmospheric Administration. 1992.
8. Rios-Berrios R, Torn RD. Climatological analysis of tropical cyclone intensity changes under moderate vertical wind shear. Mon Wea Rev. 2017;145(5):1717–38. https://doi.org/10.1175/MWR-D-16-0350.1
9. Chang M, Ho CH, Park MS, Kim J, Ahn MH. Multiday evolution of convective bursts during western North Pacific tropical cyclone development and nondevelopment using geostationary satellite measurements. J Geophys Res Atmos. 2017;122(3):1635–49. https://doi.org/10.1002/2016JD025535
10. Nam CC, Bell MM, Tao D. Bifurcation points for tropical cyclone genesis and intensification in sheared and dry environments. J Atmos Sci. 2023;80(9):2239–59. https://doi.org/10.1175/JAS-D-22-0100.1
11. Rios-Berrios R, Finocchio PF, Alland JJ, Chen X, Fischer MS, Stevenson SN, et al. A review of the interactions between tropical cyclones and environmental vertical wind shear. J Atmos Sci. 2024;81(4):713–41. https://doi.org/10.1175/JAS-D-23-0022.1
12. Park D-SR, Ho C-H, Chan JCL, Ha K-J, Kim H-S, Kim J, et al. Asymmetric response of tropical cyclone activity to global warming over the North Atlantic and western North Pacific from CMIP5 model projections. Sci Rep. 2017;7:41354. https://doi.org/10.1038/srep41354 PMID: 28134343
13. Rios-Berrios R. Impacts of radiation and cold pools on the intensity and vortex tilt of weak tropical cyclones interacting with vertical wind shear. J Atmos Sci. 2020;77(2):669–89. https://doi.org/10.1175/JAS-D-19-0159.1
14. Molinari J, Vollaro D. Rapid intensification of a sheared tropical storm. Mon Wea Rev. 2010;138(10):3869–85. https://doi.org/10.1175/2010MWR3378.1
15. Reasor PD, Eastin MD. Rapidly intensifying Hurricane Guillermo (1997). Part II: Resilience in shear. Mon Wea Rev. 2012;140(2):425–44. https://doi.org/10.1175/MWR-D-11-00080.1

16. Schecter DA. Distinct intensification pathways for a shallow-water vortex subjected to asymmetric “diabatic” forcing. Dynamics of Atmospheres and Oceans. 2020;91:101156. https://doi.org/10.1016/j.dynatmoce.2020.101156
17. Tao D, Zhang F. Effect of environmental shear, sea-surface temperature, and ambient moisture on the formation and predictability of tropical cyclones: An ensemble-mean perspective. J Adv Model Earth Syst. 2014;6(2):384–404. https://doi.org/10.1002/2014ms000314
18. Rios-Berrios R, Davis CA, Torn RD. A hypothesis for the intensification of tropical cyclones under moderate vertical wind shear. J Atmos Sci. 2018;75(12):4149–73. https://doi.org/10.1175/JAS-D-18-0070.1
19. Ryglicki DR, Doyle JD, Jin Y, Hodyss D, Cossuth JH. The unexpected rapid intensification of tropical cyclones in moderate vertical wind shear. Part II: Vortex tilt. Mon Wea Rev. 2018;146(11):3801–25. https://doi.org/10.1175/MWR-D-18-0021.1
20. Ryglicki DR, Cossuth JH, Hodyss D, Doyle JD. The unexpected rapid intensification of tropical cyclones in moderate vertical wind shear. Part I: Overview and observations. Mon Wea Rev. 2018;146(11):3773–800. https://doi.org/10.1175/MWR-D-18-0020.1
21. Ryglicki DR, Doyle JD, Hodyss D, Cossuth JH, Jin Y, Viner KC, et al. The unexpected rapid intensification of tropical cyclones in moderate vertical wind shear. Part III: Outflow–environment interaction. Mon Wea Rev. 2019;147(8):2919–40. https://doi.org/10.1175/MWR-D-18-0370.1
22. Rios-Berrios R, Torn RD, Davis CA. An ensemble approach to investigate tropical cyclone intensification in sheared environments. Part I: Katia (2011). J Atmos Sci. 2016;73(1):71–93. https://doi.org/10.1175/JAS-D-15-0052.1
23. Rios-Berrios R, Torn RD, Davis CA. An ensemble approach to investigate tropical cyclone intensification in sheared environments. Part II: Ophelia (2011). J Atmos Sci. 2016;73(4):1555–75. https://doi.org/10.1175/JAS-D-15-0245.1
24. Finocchio PM, Rios-Berrios R. The intensity- and size-dependent response of tropical cyclones to increasing vertical wind shear. J Atmos Sci. 2021;78(11):3673–90. https://doi.org/10.1175/JAS-D-21-0126.1
25. Fischer MS, Reasor PD, Rogers RF, Gamache JF. An analysis of tropical cyclone vortex and convective characteristics in relation to storm intensity using a novel airborne Doppler radar database. Mon Wea Rev. 2022;150(9):2255–78.https://doi.org/10.1175/MWR-D-21-0223.1
26. Rajasree VPM, Cao X, Ramsay H, Núñez Ocasio KM, Kilroy G, Alvey GRI, et al. Tropical cyclogenesis: controlling factors and physical mechanisms. Trop Cycl Res Rev. 2023;12(3):165–81. https://doi.org/10.1016/j.tcrr.2023.09.004
27. Persing J, Montgomery MT, Tuleya RE. Environmental interactions in the GFDL hurricane model for Hurricane Opal. Mon Wea Rev. 2002;130(2):298–317. https://doi.org/10.1175/1520-0493(2002)130<0298:EIITGH>2.0.CO;2
28. Leroux MD, Plu M, Barbary D, Roux F, Arbogast P. Dynamical and physical processes leading to tropical cyclone intensification under upper-level trough forcing. J Atmos Sci. 2013;70(8):2547–65. https://doi.org/10.1175/JAS-D-12-0293.1
29. Montgomery MT, Kilroy G, Smith RK, Črnivec N. Contribution of mean and eddy momentum processes to tropical cyclone intensification. Q J R Meteorol Soc. 2020;146(732):3101–17. https://doi.org/10.1002/qj.3837
30. Smith RK, Montgomery MT. The rotating-convection paradigm. Tropical Cyclones. Elsevier. 2023. 239–56. https://doi.org/10.1016/b978-0-44-313449-4.00019-9
31. Chu JH, Levine A, Daida S, Schiber D, Fukada E, Sampson CR. Western North Pacific ocean best track data [Internet]. Stennis Space Center (MS): Joint Typhoon Warning Center; 2025 https://www.metoc.navy.mil/jtwc/jtwc.html?western-pacific
32. Hersbach H, Bell B, Berrisford P, Hirahara S, Horányi A, Muñoz Sabater J, et al. Q J R Meteorol Soc. 2020;146(730):1999–2049. https://doi.org/10.1002/qj.3803
33. Hersbach H, Bell B, Berrisford P, Biavati G, Horányi A, Muñoz Sabater J, et al. ERA5 hourly data on pressure levels from 1940 to present. Copernicus Climate Change Service (C3S) Climate Data Store (CDS). 2023. https://doi.org/10.24381/cds.bd0915c6
34. Huang B, Liu C, Banzon V, Freeman E, Graham G, Hankins B, et al. Improvements of the Daily Optimum Interpolation Sea Surface Temperature (DOISST) Version 2.1. J Clim. 2021;34(8):2923–39. https://doi.org/10.1175/jcli-d-20-0166.1
35. National Centers for Environmental Information. Optimum interpolation sea surface temperature (OISST). https://www.ncei.noaa.gov/products/optimum-interpolation-sst 2026. 2026 February 13.
36. DeMaria M, Kaplan J. Statistical hurricane intensity prediction scheme (SHIPS) for the Atlantic basin. Wea Forecasting. 1994;9(2):209–20. https://doi.org/10.1175/1520-0434(1994)009<0209:ASHIPS>2.0.CO;2
37. Galarneau TJ Jr, Davis CA. Diagnosing forecast errors in tropical cyclone motion. Mon Wea Rev. 2013;141(2):405–30. https://doi.org/10.1175/MWR-D-12-00071.1
38. DeMaria M, Mainelli M, Shay LK, Knaff JA, Kaplan J. Further improvements to the statistical hurricane intensity prediction scheme (SHIPS). Wea Forecasting. 2005;20(4):531–43. https://doi.org/10.1175/waf862.1
39. Kruskal WH, Wallis WA. Use of ranks in one-criterion variance analysis. J Am Stat Assoc. 1952;47(260):583–621. https://doi.org/10.1080/01621459.1952.10483441
40. Wilcoxon F. Individual Comparisons by Ranking Methods. Biometrics Bulletin. 1945;1(6):80. https://doi.org/10.2307/3001968
41. Yu CL, Tang B, Fovell RG. Tropical cyclone tilt and precession in moderate shear: Precession hiatus in a critical shear regime. J Atmos Sci. 2023;80(3):909–32. https://doi.org/10.1175/JAS-D-22-0200.1
42. Zhang F, Tao D. Effects of vertical wind shear on the predictability of tropical cyclones. J Atmos Sci. 2013;70(3):975–83. https://doi.org/10.1175/JAS-D-12-0133.1

43. Dare RA, McBride JL. The threshold sea surface temperature condition for tropical cyclogenesis. J Clim. 2011;24(17):4570–6. https://doi.org/10.1175/JCLI-D-10-05006.1
44. McTaggart-Cowan R, Davies EL, Fairman JGJ, Galarneau TJJ, Schultz DM. Revisiting the 26.5°C sea surface temperature threshold for tropical cyclone development. Bull Am Meteorol Soc. 2015;96(11):1929–43. https://doi.org/10.1175/BAMS-D-13-00254.1
45. Park D-SR, Seo E, Lee M, Cha D-H, Kim D, Ho C-H, et al. Sea surface temperature warming to inhibit mitigation of tropical cyclone destructiveness over East Asia in El Niño. npj Clim Atmos Sci. 2024;7(1). https://doi.org/10.1038/s41612-023-00556-3
46. Montgomery MT, Lussier LLIII, Moore RW, Wang Z. The genesis of Typhoon Nuri as observed during the Tropical Cyclone Structure 2008 (TCS-08) field experiment – Part 1: The role of the easterly wave critical layer. Atmos Chem Phys. 2010;10(20):9879–900. https://doi.org/10.5194/acp-10-9879-2010
47. Nam CC, Bell MM. Multiscale shear impacts during the genesis of Hagupit (2008). Mon Wea Rev. 2021;149(2):551–69. https://doi.org/10.1175/MWR-D-20-0133.1
48. Ritchie EA, Holland GJ. Large-scale patterns associated with tropical cyclogenesis in the western Pacific. Mon Wea Rev. 1999;127(9):2027–43. https://doi.org/10.1175/1520-0493(1999)127<2027:LSPAWT>2.0.CO;2
49. Yoshida R, Ishikawa H. Environmental factors contributing to tropical cyclone genesis over the western North Pacific. Mon Wea Rev. 2013;141(2):451–67. https://doi.org/10.1175/MWR-D-11-00309.1
50. Wu L, Su H, Zeng X, Posselt DJ, Wong S, Chen S, et al. Uncertainty of atmospheric winds in three widely used global reanalysis datasets. J Appl Meteorol Climatol. 2024;63(2):165–80. https://doi.org/10.1175/JAMC-D-22-0198.1
51. Kosaka Y, Kobayashi S, Harada Y. The JRA-3Q reanalysis. J Meteorol Soc Jpn. 2024;102(1):49–109. https://doi.org/10.2151/jmsj.2024-004
52. The Japanese Reanalysis for Three Quarters of a Century. Japan Meteorological Agency. https://search.diasjp.net/en/dataset/JRA3Q. 2022. 2025 December 4.
53. DeMaria M, Knaff JA, Connell BH. A Tropical Cyclone Genesis Parameter for the Tropical Atlantic. Wea Forecasting. 2001;16(2):219–33. https://doi.org/10.1175/1520-0434(2001)016<0219:atcgpf>2.0.co;2
54. Wu L, Su H, Fovell RG, Dunkerton TJ, Wang Z, Kahn BH. Impact of environmental moisture on tropical cyclone intensification. Atmos Chem Phys. 2015;15(24):14041–53. https://doi.org/10.5194/acp-15-14041-2015
55. Yoshida R, Miyamoto Y, Tomita H, Kajikawa Y. The effect of water vapor on tropical cyclone genesis: A numerical experiment of a non-developing disturbance observed in Palau 2010. J Meteorol Soc Jpn. 2017;95(1):35–47. https://doi.org/10.2151/jmsj.2017-001